

Nanoporous TiO₂/Polyion Thin-Film-Coated Long-Period Grating Sensors for the Direct Measurement of Low-Molecular-Weight Analytes

Rui-Zhu Yang,[†] Wen-Fei Dong,^{*,†} Xiang Meng,[†] Xu-Lin Zhang,[†] Yun-Lu Sun,[†] Ya-Wei Hao,[†] Jing-Chun Guo,[†] Wen-Yi Zhang,[†] Yong-Sen Yu,[†] Jun-Feng Song,[†] Zhi-Mei Qi,[‡] and Hong-Bo Sun^{*,†,§}

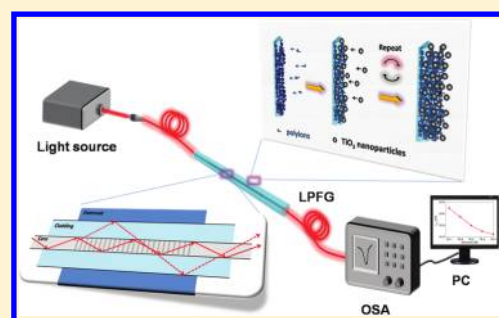
[†]State Key Laboratory on Integrated Optoelectronics, College of Electronic Science and Engineering, Jilin University, 2699 Qianjin Street, Changchun 130012, PR China

[‡]State Key Laboratory of Transducer Technology, Institute of Electronics, Chinese Academy of Sciences, Beijing 100190, PR China

[§]College of Physics, Jilin University, 119 Jiefang Road, Changchun 130023, PR China

Supporting Information

ABSTRACT: We present novel nanoporous TiO₂/polyion thin-film-coated long-period fiber grating (LPFG) sensors for the direct measurement of low-molecular-weight chemicals by monitoring the resonance wavelength shift. The hybrid overlay films are prepared by a simple layer-by-layer deposition approach, which is mainly based on the electrostatic interaction of TiO₂ nanoparticles and polyions. By the alternate immersion of LPFG into dispersions of TiO₂ nanoparticles and polyions, respectively, the so-formed TiO₂/polyion thin film exhibits a unique nanoporous internal structure and has a relative higher refractive index than LPFG cladding. In particular, the porosity of the thin film reduces the diffusion coefficient and enhances the permeability retention of low-molecular-weight analytes within the porous film. The increases in the refractive index of the LPFG overlay results in a distinguished modulation of the resonance wavelength. Therefore, the detection sensitivity of LPFG sensors has been greatly improved, according to theoretical simulation. After the structure of the TiO₂/polyion thin film was optimized, glucose solutions as an example with a low concentration of 10⁻⁷ M was easily detected and monitored at room temperature.



1. INTRODUCTION

Low-molecular-weight analytes, especially those with molecular weights of less than 300 Da, have been paid a great amount of attention because they play important roles in the quality and safety of health, food, and the environment.^{1–4} In this respect, interest in the development of rapid, in situ, portable, and cost-effective analytical tools for detecting and monitoring small molecules had been rapidly increasing over the last 10 years.^{5–9} Owing to their unique properties of low cost, easy production, miniature size, immunity to electromagnetic interference, noncorrosiveness, remote operation, and high reliability, long-period fiber grating (LPFG)-based optical sensors have become one of the best technologies of choice.^{8–11}

As shown in Scheme 1, LPFG relies on the periodic refractive index (RI) modulation of a single-mode optical fiber core and couples light from a guided-core mode into forward-propagating cladding modes. The wavelength dependence of coupling from the guided-core mode to cladding modes results in a spectrum-selective loss, called attenuation bands. The central wavelength of the attenuation bands can be described by

$$\lambda_{\text{res}} = (n_{\text{co}}^{\text{eff}} - n_{\text{cl},m}^{\text{eff}})\Lambda \quad (1)$$

where Λ is the period of the grating, λ_{res} is the central wavelength of the m th attenuation band, $n_{\text{co}}^{\text{eff}}$ and $n_{\text{cl},m}^{\text{eff}}$ are the effective RIs of the guided core mode and the m th cladding mode, respectively. For a given LPFG with fixed Λ and $n_{\text{co}}^{\text{eff}}$ (i.e., $n_{\text{core}} \approx 1.4681$, $r_{\text{core}} \approx 4.15 \mu\text{m}$ for silica), λ_{res} strongly depends on $n_{\text{cl}}^{\text{eff}}$, which is a function of both the RI of the environment (n_{en}) and the cladding radius. In theory, if Λ is 500 μm and the spectrometer resolution is 0.05 nm, then RI changes of 10⁻⁶–10⁻⁷ can be easily distinguished. For this reason, LPFG has been regarded as a novel RI sensor for measuring the RI of specific solutions and determining the relevant concentration.^{8–14}

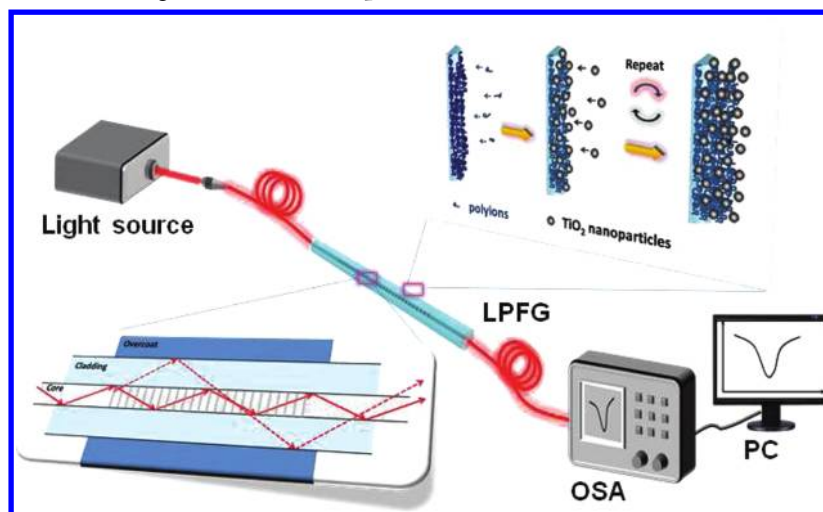
However, the poor detection sensitivity of LPFG sensors has often been observed during the measurements of low analyte solution concentrations. It is mainly due to the RI mismatch effect between n_{en} and n_{cl} of LPFG sensors.^{9–11} In general, a higher detection sensitivity of LPFG can be achieved when n_{en} is close to n_{cl} . If n_{en} is far from n_{cl} , then the sensing sensitivities will be highly suppressed.

Received: July 30, 2011

Revised: May 16, 2012

Published: May 17, 2012

Scheme 1. Experimental Setup for Nanoporous-Film-Coated LPFG Sensors and Schematic Illustration of the ESA Deposition Process and Transformation of the Light Transmission Spectrum



To overcome this problem and measure a low analyte concentration, one low-cost method is the deposition of thin film overlays with higher RI (HRI, $n_{ov} > n_{cl}$) on the fiber surface.^{15–17} By using a higher RI overlay, n_{en}^{eff} can be facilely tuned to be close to n_{cl} . It can result in a sharp shift of λ_{res} and improve the detection sensitivity of LPFG sensors.^{18–22} There are numerous methods for the deposition of the HRI overlay on the fiber surface, for instance, Langmuir–Blodgett (LB), electrostatic self-assembly (ESA), dip-coating, and sol–gel reactions.^{18–22} Among these, the ESA method has been paid more attention mainly because of its easy fabrication, precise thickness control, and flexibility with respect to the choice of substrates and overlay materials. The typical ESA process is shown in Scheme 1.^{23–29} These thin films are fabricated by alternatively immersing a charged substrate into aqueous solutions of oppositely charged materials, followed by several rinsing and air-drying steps. It had been demonstrated that LPFG coated with ESA films was more sensitive to these high-molecular-weight analytes. For example, Wang et al. reported that a low concentration of streptavidin solution (lower than 12.5 mg/L) had been detected using (PAH/PCBS)_n-coated LPFG, where PAH is poly(allyamine hydrochloride), PCBS is poly{1-[4-(3-carboxy-4-hydroxyphenylazo)-benzenesulfonamido]-1,2-ethanediyl}, and *n* is the number of bilayers.¹³ However, for these low-molecular-weight analytes (i.e. salt, ion, or sugar), the detection sensitivity of modified LPFG is not as high as expected.^{19,20} For instance, by using LPFG sensors with overlays of (PSS/PAH)₁₅₀, where PSS is poly(sodium-*p*-styrenesulfonate), the low limitation of detection of the sucrose concentration was about 10^{−3} M (5%).¹⁹ It is difficult to measure a lower concentration (~10^{−6} M) of sucrose solution.

To explain such a poor detection sensitivity, two factors are generally accepted. First, the RI of the thin-film overlay is not high enough. As compared to fiber cladding of $n_{cl} \approx 1.463$, $n_{(PSS/PAH)}$ is about 1.50,²⁰ so it is difficult to distinguish the change in λ_{res} according to eq 1. Second, the ESA film of (PSS/PAH)_n is rather smooth and has a relative small mesh size (~1 nm), which can allow only the penetration of water and ions.^{30–32} However, low-molecular-weight species, especially noncharged species of glucose, cannot penetrate the films because of the size effect so that they can stay on the overlay surface. Because the number of molecules attached to the ESA

thin-film overlay is insufficient, the detection sensitivity of LPFG is strongly suppressed.

In view of these points, the development of ESA films with higher RI^{16–18,33} and suitable porosity^{21,22} should be the prerequisites. To this end, a novel LPFG sensor is designed and fabricated for the direct measurement of low-molecular-weight analytes at a lower concentration. Robust thin films of TiO₂ nanoparticles/polyions are prepared by an ESA approach and integrated on the fiber surface as sensitive layers. The so-prepared hybrid thin films do not only have higher RI values but also contain nanoporous structures, as compared to polymeric ESA films. These advantages are helpful in realizing a high sensitivity for low-chemical-concentration detection.

2. EXPERIMENTAL SECTION

2.1. Materials. Titanium iso-propoxide, acetic acid, nitric acid (65%), ethanol, PAH ($M_w = 70\,000$ g/mol), PSS ($M_w = 70\,000$ g/mol), PDDA ($M_w = 100\,000$ g/mol), NaOH, NH₄OH, H₂O₂, R6G, HF, and isopropanol were purchased from Aldrich. Water used in all experiments was purified in a three-stage Milli-Q Plus 185 purification system and had an initial resistivity that was greater than 18.2 MΩ cm.

2.2. Fabrication of a Long-Period Fiber Grating. Single-mode fiber (Corning SMF-28ie) was purchased from Corning Company with a core diameter of 8.25 μm and a cladding diameter of 125 μm to fabricate an LPFG.^{34–39} Prior to the fabrication of LPFG, the fiber was hydrogen loaded for more than 1 month at room temperature and 100 atm and then exposed to a UV laser through a mask of period $\Lambda = 460$ μm and a total length of $L = 45$ mm. The laser that we used was a UV KrF excimer laser (Lumonics PM886) that has a wavelength of 248 nm. Consequently, the fiber was annealed for 10 h at 80 °C for the stabilization of the grating. Then we used a 40% HF aqueous solution to etch the fiber cladding from 125 μm to ~114 μm, and a grating with wavelengths at 1490 and 1587 nm was generated.

2.3. Preparation of TiO₂ Nanoparticles. The TiO₂ nanoparticles were obtained with the hydrothermal synthesis method.^{40,41} In general, 12 g (0.2 mol) of acetic acid was added to a round-bottomed flask containing 58.6 g (0.2 mol) of titanium isopropoxide drop by drop with stirring. Fifteen minutes later, the mixture was moved into 200 mL of distilled water, and immediately a white precipitate was formed. The solution was stirred vigorously for another 1 h to complete the hydrolysis. Then 4 mL of nitric acid (65%) was added. The mixture was heated to 78 °C slowly over 40 min and kept at this temperature for 75 min to obtain a homogeneous gel solution. Cold distilled water was added to the solution to cool it, and the total volume was adjusted to 370 mL. Then the mixture was moved into a

500 mL autoclave and kept at 250 °C for 12–14 h. Nitric acid (2.4 mL, 65%) was added, and the mixture was put into an ultrasonic machine to disperse the solute well. Rotary evaporation was employed to condense it to a constant weight containing 10% (w/w) TiO₂. The residual nitric acid was removed using a centrifuge, and the solution was washed with ethanol and water three times to obtain a colloidal solution containing 20% TiO₂ in water.

2.4. Preparation of a TiO₂/Polyion Film and the Dye-Loading Experiment. The TiO₂/polyion film was fabricated via the electronic self-assembly (ESA) technique. The driving force for film formation is based mainly on the electrostatic interaction between nanoparticles and polyions. The ESA deposition process for the fabrication of TiO₂/polyion is described as follows: The substrates (silica or fiber) were hydrophilized by pretreatment using water, ammonia, and hydrogen peroxide (5:1:1) for 10 h and then cleaned with ultrapure water. Then PDDA ((poly(dimethyl diallyl ammonium chloride), pH ~7, 1 mg/mL) was deposited on the clean hydrophilic substrate to achieve enough charge density prior to the self-assembly of thin films. For an example of the preparation of (TiO₂/PAH)_n films, the freshly cleaned substrate covered with a thin layer of PDDA was alternately immersed into a solution of TiO₂ nanoparticles (pH ~11.0, 3 mg/mL) and a positively charged PAH solution (pH ~7, 1 mg/mL, 0.5 M NaCl) for 10 min each time, with several intermediate water washings. The immersion and rinsing steps above were repeated until the desired layer number was reached. The growth process characterized by a UV–vis absorption spectrum is shown in the Supporting Information, Figure S1. Similarly, the preparation of (TiO₂/PSS)_n multilayers is mostly the same except for the sequence of the layers as PDDA–PSS–TiO₂–(PSS–TiO₂)_n– because PAH and PSS (pH ~7, 1 mg/mL, 0.5 M NaCl) carry opposite charges.

Dye-loading experiments were carried out to provide evidence for the porosity of the TiO₂/polyion film. Freshly prepared (PSS/TiO₂)_n films (*n* = 5, 10, 15, and 20) on a 1 × 10 × 35 mm³ silica substrate were first immersed in an R6G solution of 1 mM in isopropanol at 70 °C to allow the diffusion and penetration of dye. After 12 h, the films were then taken out and rinsed with Millipore water several times until no dyes stayed on the surface. The washing step is important because it could allow the solvent effect on the hybrid film to be avoided. For dye desorption, fresh isopropanol was used to extract the dye from the hybrid film.

2.5. Glucose Molecule Loading and Detecting. For the final detection application of low-molecular-weight materials such as noncharged species of glucose in aqueous solution, the nanoporous thin film was coated onto LPFG. The measurements were conducted with the system in Scheme 1 for a glucose solution concentration varying from 10⁻³ to 10⁻⁷ M. Nanoporous-film-coated LPFG was immersed and kept in the aqueous glucose solution at room temperature for 2 min until the transmission spectra were stable. Then the glucose-loaded LPFG was removed and rinsed with Millipore water several times until there were no free glucose molecules on the surface of the overlay film. Then the transmission spectrum of LPFG was measured with an optical spectrum analyzer (OSA, Ando AQ-6315A) with 0.05 nm of resolution at 15 (±0.1) °C. Here it should be mentioned that all of the film growth and optical measurements should be carried out in aqueous solution in order to achieve a stable inner structure of the hybrid film. To make a comparison, the pure LPFG sensors were tested for detection under the same condition.

2.6. Characterization. Transmission electron microscope (TEM) photographs were taken on a JEOL JEM-2000FX microscope equipped with a Link AN10000 EDX spectrometer and a Gatan TV camera. TiO₂ nanoparticles were supported on holey carbon films mounted on Cu grids. More than 100 particles for each sample were counted for particle size distribution measurements and average size calculations. The X-ray diffraction patterns were acquired on a Rigaku X-ray diffractometer operated at 45 kV and 40 mA with Cu K α radiation (1.5418 Å) and a diffracted-beam monochromator. Scanning electron microscope (SEM) photographs were taken by SEM (JSM 7500F, JEOL, Tokyo, Japan) at an operating voltage of 5.0 keV.

Ultraviolet–visible (UV–vis) spectra were recorded using a Shimadzu UV-2550 spectrophotometer.

3. RESULTS AND DISCUSSION

3.1. Self-Assembled TiO₂/Polyion Hybrid Thin Film.

The morphology of the hydrothermally synthesized TiO₂ nanoparticles is shown in the TEM in Figure 1, where as-

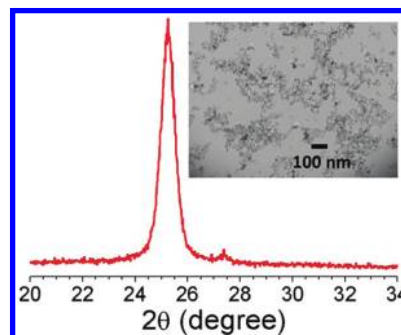


Figure 1. XRD pattern of powder TiO₂ nanocrystals. (Inset) TEM image of synthesized TiO₂ nanoparticles, average diameter ~30 nm.

synthesized TiO₂ nanoparticles are diamondlike and have a grain size of around 24.0 nm. The XRD results in Figure 1 indicate that these TiO₂ nanoparticles have polycrystalline structure. Most of them are anatase with a peak at 25.5°, and only a small part are rutile with a peak at 27.5°.

The surface charge of TiO₂ nanoparticles strongly depends on the pH value of the solution. Because its isoelectric point is around 5.8, positively charged TiO₂ nanoparticles can be obtained by adjusting the pH to 3.0; in contrast, a negative charge will be achieved at pH ~11.0. Because of the unique amphoteric behavior of TiO₂ nanoparticles, ESA films can be prepared by self-assembly with different polyions (PAH or PSS).^{42–46}

The structure of the LPFG coated with the TiO₂/polyion hybrid thin film is illustrated in Figure 2a, and the refractive index profile is shown as well. Prior to film deposition, charged substrates (i.e., optical fibers) have to be modified with a thin layer of PDDA or PEI (poly(ethylenimine)) in order to achieve enough charge density. The film-formation process can be easily monitored by UV–vis spectroscopy or QCM measurements (Supporting Information, Figure S1).^{43–47} The thickness of the TiO₂/polyion hybrid thin film is facilely controlled by the number of bilayers. According to AFM measurements described in the literature, the single-bilayer thicknesses of TiO₂/PAH and PSS/TiO₂ are estimated to be ~36.0 and ~14.4 nm for the 24.0 nm nanoparticles,^{42,44} respectively. The bilayer thickness of (TiO₂/PAH)_n that was used to coat LPFG is measured as 32.86 nm, close to the estimated value (data shown in Supporting Information, Figure S2).

Until the desired thickness (or number of bilayers) is reached, the surface morphology of (TiO₂/polyion)_n thin films is characterized by SEM. As shown in Figure 2, the surface roughness is very high and many nanoparticle aggregations can be identified, which are totally different from those of smooth polymeric ESA films (i.e., (PSS/PAH)_n or (PSS/PDDA)_n).^{21,22} Here we should mention that the self-assembly profiles of the ESA film are not influenced by the shape of the substrate because the surface area of LPFG is large enough. Similar morphology can be observed in films of either (PSS/TiO₂)₁₀ or (TiO₂/PAH)₁₀, as compared to Figure 2b,c. This demonstrates

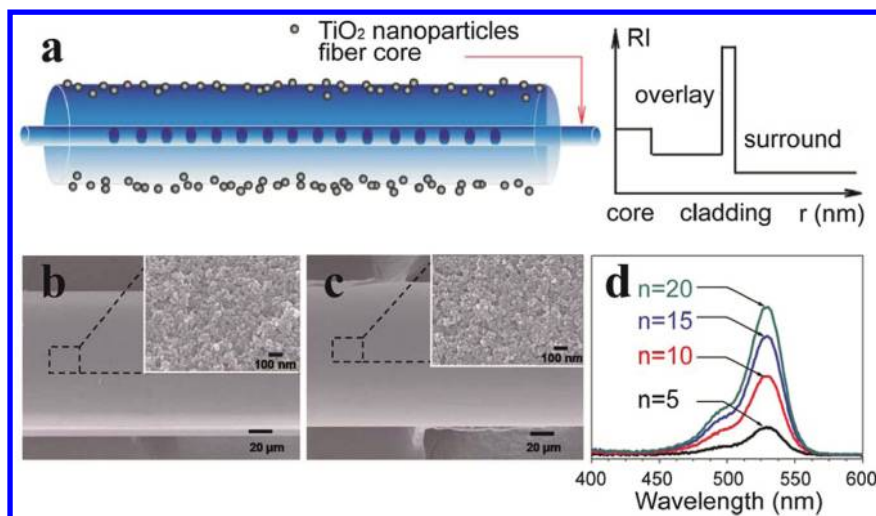


Figure 2. (a) Scheme of a nanoporous-thin-film-coated LPFG and the index profile of LPFG. Topographic SEM images of LPFG coated with films of (b) $(\text{TiO}_2/\text{PAH})_{10}$ and (c) $(\text{PSS}/\text{TiO}_2)_{10}$. (d) UV spectra of extracted R6G dye solution from a dye-loaded nanoporous film of $(\text{PSS}/\text{TiO}_2)_n$ ($n = 5, 10, 15,$ and 20).

that the film structure of $(\text{TiO}_2/\text{polyion})_{10}$ is independent of the linear polyions, in agreement with Kirstein's results.^{43,44} However, larger TiO_2 nanoparticles may result in an increase in surface roughness.

As is well known, the surface roughness of films could be related to their internal nanostructure. The large distance (>50 nm, data shown in Supporting Information, Figure S3) between particle aggregations indicates the porous nature of hybrid films, which can be demonstrated by dye adsorption/desorption experiments. If the film is smooth or has a small mesh size, then most of the dye will be anchored on the surface. Therefore, the concentration of dye in the film will not depend on the film thickness. However, if the film has a large mesh size, then the concentration of dye will increase with increasing film thickness (or an increasing number of bilayers). The dye adsorption/desorption behavior is monitored by the UV-vis spectrum. In the Supporting Information, we show the UV-vis spectra of R6G dye-loaded nanoporous films. As compared to the UV spectrum of free R6G solution, the typical R6G absorption peak at 450–550 nm can be observed in the dye-loaded films (Figure S4). Because R6G has a weak charge, it is difficult to immigrate from film to solution. For dye desorption, we used fresh isopropanol to extract the dye in the hybrid film. The concentration of R6G in the extraction solution is measured by the UV-vis spectrum. As shown in Figure 2d, we found that the dye concentration increases with the number of bilayers. These results confirm that the $\text{TiO}_2/\text{polyion}$ film has a porous structure that can allow the penetration of some small organic molecules such as R6G.

As is well known, porosity plays an important role in the RI value of a TiO_2 film. Normally, RI values of nanoporous films can be estimated by eq 2:⁴⁸

$$\phi_{\text{TiO}_2} \frac{n_{\text{TiO}_2}^2 - n_{\text{hybrid}}^2}{n_{\text{TiO}_2}^2 + 2n_{\text{hybrid}}^2} + (1 - \phi_{\text{TiO}_2}) \frac{n_{\text{air}}^2 - n_{\text{hybrid}}^2}{n_{\text{air}}^2 + 2n_{\text{hybrid}}^2} = 0 \quad (2)$$

Here, n_{TiO_2} and n_{air} represent the RIs of the two components, TiO_2 ($n \approx 2.5$, anatase) and air ($n \approx 1.0$), respectively, and ϕ_{TiO_2} is the porosity ratio of TiO_2 nanoparticles. Within the

nanoporous film, the random distribution of TiO_2 nanoparticles can be easily observed. Therefore, ϕ_{TiO_2} will fall into the regime between regular accumulation (0.524) and close packing (0.698). If the algebraic mean value is taken, then ϕ_{TiO_2} is assumed to be 0.611. Then we can estimate n_{hybrid} to be about 1.89, which is much higher than those of polymeric ESA films. As was demonstrated by Cohen's work, the RI value of the PSS/TiO_2 film was about 1.75–1.91,^{45–47} which agrees well with our assumption.

3.2. Structure Effect on Detecting the Sensitivity of LPFGs. In general, the value of $\Delta\lambda_{\text{res}}/\Delta n$ is often used to evaluate the detection sensitivity of LPFG. After the HRI thin-film overlay is used in coating, the detection sensitivity of LPFG could be influenced by n_{ov} and the overlay thickness (d_{ov}) for the appropriate choice of cladding-mode order. To optimize the structure of the overlay for low-molecular-weight-analyte measurement, we will first investigate the influence of these parameters on the detection sensitivity of LPFG in theory.

The propagation of light in the LPFG is represented by the coupled-mode equations⁴⁹ as follows:

$$\begin{aligned} \frac{dA^{\text{co}}}{dz} &= i\kappa_{01-01}^{\text{co-co}} A^{\text{co}} + i \sum_{\nu} \frac{m}{2} \kappa_{1\nu-01}^{\text{cl-co}} A_{\nu}^{\text{cl}} \exp(-i2\delta_{1\nu-01}^{\text{cl-co}} z) \\ \sum_{\nu} \left[\frac{dA_{\nu}^{\text{cl}}}{dz} &= +i \frac{m}{2} \kappa_{1\nu-01}^{\text{cl-co}} A^{\text{co}} \exp(+i2\delta_{1\nu-01}^{\text{cl-co}} z) \right] \end{aligned} \quad (3)$$

The parameters in the equations are interpreted as follows: A^{co} , amplitude of the core mode; A_{ν}^{cl} , amplitude of the ν th cladding mode; z , propagation direction; m , induced-index fringe modulation; $\kappa_{01-01}^{\text{co-co}}$, core-mode–core-mode coupling constant; $\kappa_{1\nu-01}^{\text{cl-co}}$, core-mode–cladding-mode coupling constant; and $\delta_{1\nu-01}^{\text{cl-co}}$, small-detuning parameter. Here we do not take the transmission spectra into account, but we do consider λ_{res} from which we can easily find our fiber's sensitivity to the ambient refractivity. λ_{res} can be approximately calculated by

$$\delta_{1\nu-01}^{\text{cl-co}} + \frac{\kappa_{01-01}^{\text{co-co}}}{2} = 0 \quad (4)$$

$$\delta_{1\nu-01}^{cl-co} = \frac{1}{2} \left(\beta_{01}^{co} - \beta_{1\nu}^{cl} - \frac{2\pi}{\Lambda} \right) \quad (5)$$

β_{01}^{co} is the propagation of the core mode and $\beta_{1\nu}^{cl}$ is the ν order cladding mode, Λ is the period of the grating. κ is the core-mode-core-mode coupling constant which is defined by:

$$\kappa_{01-01}^{co-co} = \frac{\omega \epsilon_0 n_{core}^2 \sigma(z)}{2} \int_0^{2\pi} d\phi \int_0^{r_{core}} r dr (|E_r^{co}|^2 + |E_\phi^{co}|^2) \quad (6)$$

ω is the frequency; ϵ_0 is the permittivity of free space; n_{core} is the core refractive index; $\sigma(z)$ is the slowly varying envelope of the grating; r_{core} is the core radius; E_r^{co} and E_ϕ^{co} are the core-mode normalized electric fields in r and ϕ directions, respectively. We first calculated the λ_{res} between the core mode and the third cladding mode under different n_{ov} and thicknesses, where our simulation parameters are $n_{core} = 1.4681$, $n_{cl} = 1.4573$, core radius = $4.15 \mu\text{m}$, cladding radius = $57 \mu\text{m}$, and period = $460 \mu\text{m}$. Then we calculated the detection sensitivity ($\Delta\lambda_{res}/\Delta n$) as a function of n_{ov} and d_{ov} . The corresponding results are given in Figure 3a.

As shown in Figure 3a, the upheaval area indicates the region with high sensitivity. From it we could find that for a fixed n_{ov} , there is always a most-sensitive region at some overlay

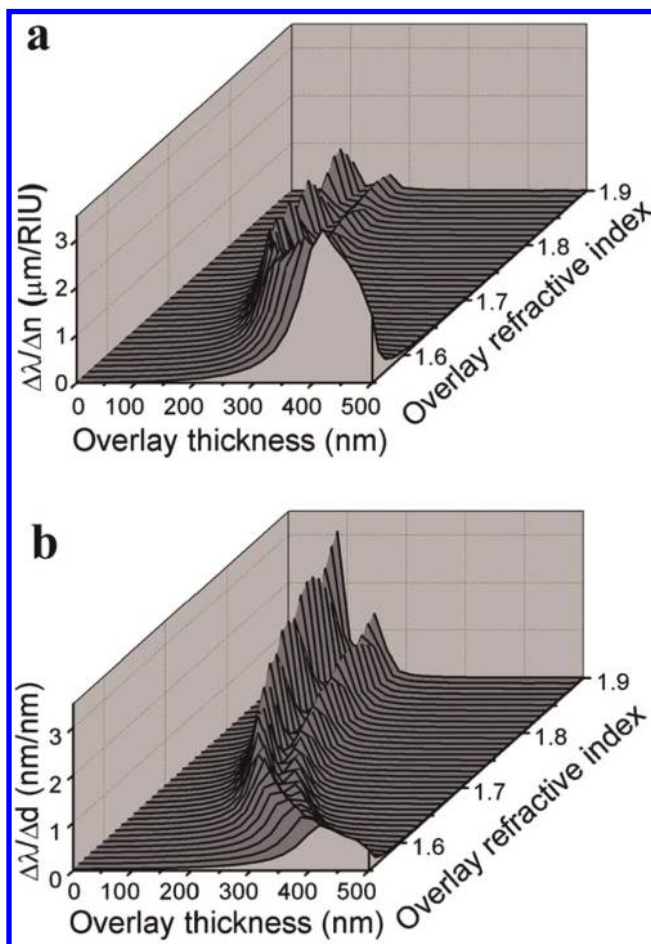


Figure 3. Theoretical simulated (a) $\Delta\lambda_{res}/\Delta n$ and (b) $\Delta\lambda_{res}/\Delta d$ as functions of n_{ov} and d_{ov} with parameters as follows: $n_{core} \approx 1.4681$, $n_{cl} \approx 1.463$, core radius $\approx 4.15 \mu\text{m}$, cladding radius $\approx 57 \mu\text{m}$, and period $\approx 460 \mu\text{m}$.

thickness where the equivalent average RI of the overlay and ambient medium is closest to that of the grating cladding. Otherwise, the detection sensitivity is strongly suppressed while the overlay thickness d_{ov} is higher or lower.

However, if n_{ov} is higher, the highest sensitivity of LPFGs may take place at a thinner overlay. That is the reason that the HRI thin-film overlay has the ability to achieve a higher detection sensitivity. Otherwise, if n_{ov} is lower, then the thicker overlay will result in a higher detection sensitivity. Concerning the easy fabrication of the overlay film, the latter case is not suitable for further fabrication. Thus, using the HRI thin film as the overlay is the best choice for achieving a higher detection sensitivity.

For a certain overlay material (n_{ov} is fixed), the overlay thickness d_{ov} is the crucial parameter to achieving a high detection sensitivity ($\Delta\lambda_{res}/\Delta n$). However, the highest sensitivity ($\Delta\lambda_{res}/\Delta n$) is difficult to achieve during the experiment and the mathematics simulation could reflect only the trend in the sensitivity influenced by n_{ov} and d_{ov} , rather than giving the exact overlay thickness corresponding to the highest-sensitivity region. Fortunately, we could ensure the detection sensitivity ($\Delta\lambda_{res}/\Delta n$) through the thickness sensitivity ($\Delta\lambda_{res}/\Delta d$). We also calculate $\Delta\lambda_{res}/\Delta d$ as function of n_{ov} and d_{ov} , as shown in Figure 3b. It also depicts that at fixed n_{ov} the best detection sensitivity can be reached by increasing the film thickness. In addition, by comparing Figure 3a,b, the best detection-sensitivity regions overlap well with each other. That indicates that when $\Delta\lambda_{res}/\Delta n$ is at its maximum, $\Delta\lambda_{res}/\Delta d$ will also be maximized as well. Thus, by simply plotting $\Delta\lambda_{res}$ as function of thickness, the best detection-sensitivity region will exist at a certain film thickness, where the value of $\Delta\lambda_{res}/\Delta n$ goes to its maximum.

On the basis of this assumption, the film thickness (or number of bilayers) should be optimized to achieve a higher detection sensitivity. In this respect, the response law of (PAH/ TiO_2)_n-coated LPFG sensors is measured at room temperature in different mediums, including air, water ($n \approx 1.3333$), ethanol ($n \approx 1.3614$), butanol ($n \approx 1.4005$), and diethylene glycol ($n \approx 1.4485$). Considering the possible influence of the organic solvents on the film thickness and structure, the coated LPFG should be marinated in the mediums for enough time during the measurement so that the film can stay in an invariable environment for every measurement. The resonant wavelength changes of coated LPFG are shown in Figure 4. For all media, λ_{res} exhibits a blue shift with increasing film thickness obviously

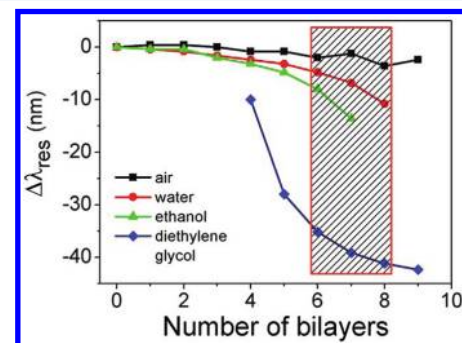


Figure 4. LPFG sensor responses to different RI media, including air ($n = 1.0$), water ($n \approx 1.3333$), ethanol ($n \approx 1.3614$), butanol ($n \approx 1.4005$), and diethylene glycol ($n \approx 1.4485$). Resonant wavelength shifts as a function of the number of bilayers.

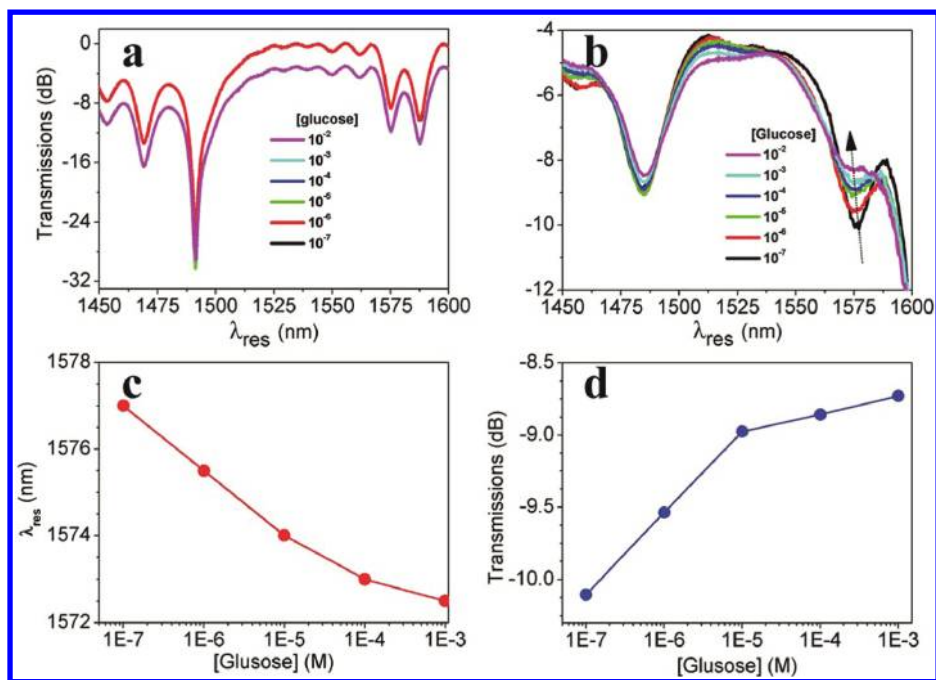


Figure 5. Comparison of the transmission spectra of LPFG (a) without a film and (b) coated with $(TiO_2/PAH)_7$ in glucose solutions with different concentrations from 10^{-3} to 10^{-7} M. (c) Resonant wavelength shifts. (d) Transmission intensities as a function of glucose concentration.

shifts at the thicker layer, in agreement with theoretical simulation. The spectra provided direct in situ monitoring of film growth. As compared to that of pure LPFG, $\Delta\lambda_{res}$ will shift 6.8 nm for $(PAH/TiO_2)_7$ -coated LPFG in water. We also found that n_{en} plays an important role in $\Delta\lambda_{res}$. At a fixed thickness of ~ 230 nm ($(PAH/TiO_2)_7$), $\Delta\lambda_{res}$ will shift 13.6 nm in ethanol and 42.4 nm in diethylene glycol.

As discussed above, the best sensing sensitive region can be evaluated by the changes in $\Delta\lambda_{res}/\Delta d$. In other words, by simply exploring the maximum value of the slope in Figure 4 one can find the optimized overlay thickness. For example, there is a sharp decrease in $\Delta\lambda_{res}$ for a thickness of ~ 230 nm (or $n = 7$) in diethylene glycol ($n \approx 1.4485$) in Figure 4, and the behavior can be observed in water ($n \approx 1.3333$) and ethanol ($n \approx 1.3614$). Thus, the results indicate that a high detection sensitivity of LPFG can be achieved if the overlay thickness is ~ 230 nm. Of course, an important point should be taken into account that the sensor must be pretreated with the corresponding background solvent when being used to detect some analytes that were dissolved in some organic solvents.

3.3. Direct Measurements of Low-Molecular-Weight Analytes. As discussed before, an overlay film with HRI and unique porosity will be helpful in improving the detection sensitivity of LPFG. In particular, the increase in the refractive index of the LPFG overlay results in a distinguished shift of the resonance wavelength, and the porosity of the thin film will reduce the diffusion coefficient and enhance the permeability retention of low-molecular-weight analytes within the porous film. Therefore, this will cause a strong resonance wavelength shift.

In this work, nanoporous-thin-film-coated LPFG sensors were utilized for the detection of low-molecular-weight materials (i.e., noncharged glucose species in aqueous solution). The measurements were conducted with the setup in Scheme 1 for concentration varying from 10^{-3} to 10^{-7} M. The film growth and optical measurement should be made in aqueous solution in order to achieve a stable inner structure of the

hybrid film.⁵⁰ According to the theoretical simulation in Figure 3 and the experimental analysis in Figure 4, the optimized overlay thickness should be about 230 nm. Because the single bilayer thickness of $(TiO_2/PAH)_n$ is ~ 32.86 nm, the optical fiber grating was coated with seven bilayers. Figure 5 presents the results of glucose measurements. For pure LPFG sensors, increasing the glucose concentration did not cause the shift in λ_{res} in Figure 5a. However, from Figure 5b, after the sensors were coated with $(TiO_2/PAH)_7$ thin films, the shift in λ_{res} toward smaller wavelength can be easily observed. λ_{res} shifted 4 nm for glucose concentration changing from 10^{-3} to 10^{-7} M. The dependence of λ_{res} and the depth of the attenuation bands with respect to the glucose concentration are also provided in Figure 5c,d, from which it can be seen that λ_{res} and the depth of the attenuation band show nearly linear correlations with the logarithm of the glucose concentration. The correlations can provide elementary references for quantitative measurement. As compared to previous results, the limiting concentration of glucose in this study is 4 orders of magnitude lower, and these unprecedented capacities of the LPFG sensor mainly result from the existence of high RI and the unique porosity of the TiO_2 /polyion thin film.

It should be noted that there are no specific interactions between glucose and the nanoporous TiO_2 /polyions thin film, which is the reason that a fast, reversible diffusion of analytes through the films could be easily observed. Also, the TiO_2 /polyion film-coated LPFG can maintain the physical and chemical states over several cycles of use. Moreover, the resulting thin film is stable and no obvious detachment was observed in either acidic or alkali solutions over several cycles of use in both acidic and alkaline solutions. The acidic (pH 1) and alkaline (pH 13) treatments are shown in the Supporting Information as Figure S5. The excellent chemical stability of thin-film-coated LPFG possibly endows the sensor with effects under some strongly acidic or basic conditions for repeated use.

4. CONCLUSIONS

We have presented a novel nanoporous TiO₂/polyion thin-film-coated long-period fiber grating (LPFG) sensor for direct measurements on low-molecular-weight chemicals by monitoring their resonance wavelength shift. Here, the hybrid overlay films were prepared by a simple layer-by-layer deposition approach that was based on the electrostatic interaction of TiO₂ nanoparticles and polyions. By the alternate dipping of LPFG into dispersions of TiO₂ nanoparticles and polyions, respectively, the film thickness was controllable on the nanometer scale. The unique porous internal structure of the TiO₂/polyion thin film was characterized by the dye adsorption/desorption measurement. An as-formed thin film had a relatively higher refractive index than that resulting from LPFG cladding. The detection sensitivity of LPFG could be greatly improved by the HRI nanoporous overlay film because the increasing refractive index of the overlay film resulted in a distinguished modulation of the resonance wavelength and the porosity of the thin film would reduce the diffusion coefficient and enhance the permeability retention of low-molecular-weight analytes within the porous film. Therefore, glucose solutions with low concentration of 10⁻⁷ M could be easily detected at room temperature after the structure of the TiO₂/polyion thin film was optimized. Such novel nanoporous TiO₂/polyion thin-film-coated LPFG sensors could fulfill the requirement of simple, inexpensive, high-resolution low-molecular-weight chemical sensing in fundamental biological research, drug screening, medical diagnostics, food quality testing, and biohazard detection.

■ ASSOCIATED CONTENT

Supporting Information

Film growth and dye loading expressed by a UV-vis spectrum. Film thickness and average distance between particle aggregations characterized by SEM. Film pH stability expressed by the transmission spectrum of LPFG. This material is available free of charge via the Internet at <http://pubs.acs.org>.

■ AUTHOR INFORMATION

Corresponding Author

*(W.-F.D.) E-mail: dongwf@jlu.edu.cn. (H.-B.S.) E-mail: hbsun@jlu.edu.cn. Tel: +49 331 567 9201. Fax: +49 331 567 9202.

Notes

The authors declare no competing financial interest.

■ ACKNOWLEDGMENTS

This work is supported by the 863 program under grant 2009AA03Z401 and by the National Science Foundation of China (grant nos. 60807030, 61077066, 91123029, 91123027, and 90923037).

■ REFERENCES

- (1) Hodnik, V.; Anderluh, G. Toxin Detection by Surface Plasmon Resonance. *Sensors* **2009**, *9*, 1339–1354.
- (2) Karlsson, R.; Stahlberg, R. Surface Plasmon Resonance Detection and Multiplex Sensing for Direct Monitoring of Interactions Involving Low-Molecular-Weight Analytes and for Determination of Low Affinities. *Anal. Biochem.* **1995**, *228*, 274–280.
- (3) Li, D.; Shlyahovskiy, B.; Elbaz, J.; Willner, I. Amplified Analysis of Low-Molecular-Weight Substrates or Proteins by the Self-Assembly of DNzyme-Aptamer Conjugates. *J. Am. Chem. Soc.* **2007**, *129*, 5804–5805.

- (4) Zhang, A.; Fang, Y. L.; Meng, J. F.; Wang, H.; Chen, S. X.; Zhang, Z. W. Analysis of Low Molecular Weight Organic Acids in Several Complex Liquid Biological Systems via HPLC with Switching Detection Wavelength. *J. Food Compos. Anal.* **2011**, *24*, 449–455.

- (5) Baker, B. R.; Lai, R. Y.; Wood, M. S.; Doctor, E. H.; Heeger, A. J.; Plaxco, K. W. An Electronic, Aptamer-Based Small-Molecule Sensor for the Rapid, Label-Free Detection of Cocaine in Adulterated Samples and Biological Fluids. *J. Am. Chem. Soc.* **2006**, *128*, 3138–3139.

- (6) Schedin, F.; Geim, A. K.; Morozov, S. V.; Hill, E. W.; Blake, P.; Katsnelson, M. I.; Novoselov, K. S. Detection of Individual Gas Molecules Adsorbed on Graphene. *Nat. Mater.* **2007**, *6*, 652–655.

- (7) Shankaran, D. R.; Gobi, K. V.; Miura, N. Recent Advancements in Surface Plasmon Resonance Immunosensors for Detection of Small Molecules of Biomedical, Food and Environmental Interest. *Sens. Actuators, B* **2007**, *121*, 158–177.

- (8) James, S. W.; Tatam, R. P. Fibre Optic Sensors with Nano-Structured Coatings. *J. Opt. A: Pure Appl. Opt.* **2006**, *8*, S430–S444.

- (9) Kim, D. W.; Zhang, Y.; Cooper, K. L.; Wang, A. In-Fiber Reflection Mode Interferometer Based on a Long-Period Grating for External Refractive-Index Measurement. *Appl. Opt.* **2005**, *44*, 5368–5373.

- (10) Wang, Z. Y.; Ramachandran, S. Ultrasensitive Long-Period Fiber Gratings for Broadband Modulators and Sensors. *Opt. Lett.* **2003**, *28*, 2458–2460.

- (11) Falciai, R.; Mignani, A. G.; Vannini, A. Fresnel-Reflection-Based Fiber Sensor for On-Line Measurement of Solute Concentration in Solutions. *Sens. Actuators, B* **2001**, *74*, 74–77.

- (12) DeLisa, M. P.; Zhang, Z.; Shiloach, M.; Pilevar, S.; Davis, C. C.; Sirkis, J. S.; Bentley, W. E. Evanescent Wave Long-Period Fiber Bragg Grating as an Immobilized Antibody Biosensor. *Anal. Chem.* **2000**, *72*, 2895–2900.

- (13) Wang, Z. Y.; Heflin, J. R.; Cott, K. V.; Stolen, R. H.; Ramachandran, S.; Ghalimi, S. Biosensors Employing Ionic Self-Assembled Multilayers Adsorbed on Long-Period Fiber Gratings. *Sens. Actuators, B* **2009**, *139*, 618–623.

- (14) Wang, Z. Y.; Xiao, H. Optical Intensity-Based Long-Period Fiber Grating Biosensors and Biomedical Applications. *Signal Processing Magazine, IEEE* **2009**, *26*, 121–122, 124–127.

- (15) Rees, N. D.; James, S. W.; Taram, R. P. Optical Fiber Long-Period Gratings with Langmuir-Blodgett Thin-Film Overlays. *Opt. Lett.* **2002**, *27*, 686–688.

- (16) Villar, I. D.; Achaerandio, M.; Matias, I. R.; Arregui, F. J. Deposition of Overlays by Electrostatic Self-Assembly in Long-Period Fiber Gratings. *Opt. Lett.* **2005**, *30*, 720–722.

- (17) Ishaq, I. M.; Quintela, A.; James, S. W.; Ashwell, G. J.; Lopez-Higuera, J. M.; Tatam, R. P. Modification of the Refractive Index Response of Long Period Gratings Using Thin Film Overlays. *Sens. Actuators, B* **2005**, *107*, 738–741.

- (18) Cusano, A.; Pilla, P.; Contessa, L.; Iadicco, A.; Campopiano, S.; Cutolo, A. High-Sensitivity Optical Chemosensor Based on Coated Long-Period Gratings for sub-ppm Chemical Detection in Water. *Appl. Phys. Lett.* **2005**, *87*, 234105.

- (19) Li, Q. S.; Qian, Y.; Yu, Y. S.; Wu, G.; Sui, Z. Y.; Wang, H. Y. Actions of Sodium Nitrite on Long Period Fiber Grating with Self-Assembled Polyelectrolyte Films. *Opt. Commun.* **2009**, *282*, 2446–2450.

- (20) Li, Q. S.; Zhang, X. L.; Yu, Y. S.; Qian, Y.; Dong, W. F.; Li, Y.; Shi, J. G.; Yan, J. T.; Wang, H. Y. Enhanced Sucrose Sensing Sensitivity of Long Period Fiber Grating by Self-Assembled Polyelectrolyte Multilayers. *React. Funct. Polym.* **2011**, *71*, 335–339.

- (21) Tang, X. L.; Rimmel, K.; Lan, X. W.; Deng, J. D.; Xiao, H.; Dong, J. H. Perovskite-Type Oxide Thin Film Integrated Fiber Optic Sensor for High-Temperature Hydrogen Measurement. *Anal. Chem.* **2009**, *81*, 7844–7848.

- (22) Tang, X. L.; Provenzano, J.; Xu, Z.; Dong, J. H.; Duan, H. B.; Xiao, H. Acidic ZSM-5 Zeolite-Coated Long Period Fiber Grating for Optical Sensing of Ammonia. *J. Mater. Chem.* **2011**, *21*, 181–186.

- (23) Sun, Y. P.; Hao, E.; Zhang, X.; Yang, B.; Shen, J. C.; Chi, L. F.; Fuchs, H. Buildup of Composite Films Containing TiO₂/PbS

Nanoparticles and Polyelectrolytes Based on Electrostatic Interaction. *Langmuir* **1997**, *13*, 5168–5174.

(24) Sun, J. Q.; Wu, T.; Sun, Y. P.; Wang, Z. Q.; Zhang, X.; Shen, J. C.; Cao, W. X. Fabrication of a Covalently Attached Multilayer via Photolysis of Layer-by-Layer Self-Assembled Films Containing Diazo-Resins. *Chem. Commun.* **1998**, 1853–1854.

(25) Zhang, X.; Shi, F.; Yu, X.; Liu, H.; Fu, Y.; Wang, Z. Q.; Jiang, L.; Li, X. Y. Polyelectrolyte Multilayer as Matrix for Electrochemical Deposition of Gold Clusters: Toward Super-Hydrophobic Surface. *J. Am. Chem. Soc.* **2004**, *126*, 3064–3065.

(26) Kalsin, A. M.; Fialkowski, M.; Paszewski, M.; Smoukov, S. K.; Bishop, K. J. M.; Grzybowski, B. A. Electrostatic Self-Assembly of Binary Nanoparticle Crystals with a Diamond-like Lattice. *Science* **2006**, *312*, 420–424.

(27) Paloniemi, H.; Lukkari, M.; Aaritalo, T.; Areva, S.; Leiro, J.; Heinonen, M.; Haapakka, K.; Lukkari, J. Layer-by-Layer Electrostatic Self-Assembly of Single-Wall Carbon Nanotube Polyelectrolytes. *Langmuir* **2006**, *22*, 74–83.

(28) Thierry, B.; Zimmer, L.; McNiven, S.; Finnie, K.; Barbe, C.; Griesser, H. J. Electrostatic Self-Assembly of PEG Copolymers onto Porous Silica Nanoparticles. *Langmuir* **2008**, *24*, 8143–8150.

(29) Zhang, X.; Chen, H.; Zhang, H. Y. Layer-by-Layer Assembly: From Conventional to Unconventional Methods. *Chem. Commun.* **2007**, 1395–1405.

(30) Ma, Y. J.; Dong, W. F.; Hempenius, M. A.; Mohwald, H.; Vancso, G. J. Layer-by-Layer Constructed Macroporous Architectures. *Angew. Chem., Int. Ed.* **2007**, *46*, 1702–1705.

(31) Ma, Y. J.; Dong, W. F.; Hempenius, M. A.; Mohwald, H.; Vancso, G. J. Redox-Controlled Molecular Permeability of Composite-Wall Microcapsules. *Nat. Mater.* **2006**, *5*, 724–729.

(32) Dong, W. F.; Ferri, J. K.; Adalsteinsson, T.; Schonhoff, M.; Sukhorukov, G. B.; Mohwald, H. Influence of Shell Structure on Stability, Integrity, and Mesh Size of Polyelectrolyte Capsules: Mechanism and Strategy for Improved Preparation. *Chem. Mater.* **2005**, *17*, 2603–2611.

(33) Wang, Z. Y.; Hefflin, J. R.; Stolen, R. H.; Ramachandran, S. Analysis of Optical Response of Long Period Fiber Gratings to nm-Thick Thin-Film Coating. *Opt. Express* **2005**, *13*, 2808–2813.

(34) Vengsarkar, A. M.; Lemaire, P. J.; Judkins, J. B.; Bhatia, V.; Erdogan, T.; Sipe, J. E. Long-Period Fiber Gratings as Band-Rejection Filters. *J. Lightwave Technol.* **1996**, *14*, 58–65.

(35) Hwang, I. K.; Yun, S. H.; Kim, B. Y. Long-Period Fiber Gratings Based on Periodic Microbends. *Opt. Lett.* **1999**, *24*, 1263–1265.

(36) Savin, S.; Dignonnet, M. J. F.; Kino, G. S.; Shaw, H. J. Tunable Mechanically Induced Long-Period Fiber Gratings. *Opt. Lett.* **2000**, *25*, 710–712.

(37) Chen, K. P.; Herman, P. R.; Zhang, J.; Tam, R. Fabrication of Strong Long-Period Gratings in Hydrogen-Free Fibers with 157-nm F2-Laser Radiation. *Opt. Lett.* **2001**, *26*, 771–773.

(38) Rao, Y. J.; Wang, Y. P.; Ran, Z. L.; Zhu, T. Novel Fiber-Optic Sensors Based on Long-Period Fiber Gratings Written by High-Frequency CO₂ Laser Pulses. *J. Lightwave Technol.* **2003**, *21*, 1320–1327.

(39) Chen, C.; Yu, Y. S.; Yang, R.; Wang, L.; Guo, J. C.; Chen, Q. D.; Sun, H. B. Monitoring Thermal Effect in Femtosecond Laser Interaction with Glass by Fiber Bragg Grating. *J. Lightwave Technol.* **2011**, *29*, 2126–2130.

(40) Choi, W.; Termin, A.; Hoffmann, M. R. The Role of Metal Ion Dopants in Quantum-Sized TiO₂: Correlation between Photo-reactivity and Charge Carrier Recombination Dynamics. *J. Phys. Chem.* **1994**, *98*, 13669–13679.

(41) Wang, P.; Zakeeruddin, S. M.; Comte, P.; Charvet, R.; Humphry-Baker, R.; Gratzel, M. Enhance the Performance of Dye-Sensitized Solar Cells by Co-Grafting Amphiphilic Sensitizer and Hexadecylmalonic Acid on TiO₂ Nanocrystals. *J. Phys. Chem. B* **2003**, *107*, 14336–14341.

(42) He, J.; Mosurkal, R.; Samuelson, L. A.; Li, L.; Kumar, J. Dye-Sensitized Solar Cell Fabricated by Electrostatic Layer-by-Layer

Assembly of Amphoteric TiO₂ Nanoparticles. *Langmuir* **2003**, *19*, 2169–2174.

(43) Schulze, K.; Kirstein, S. Layer-by-Layer Deposition of TiO₂ Nanoparticles. *Appl. Surf. Sci.* **2005**, *246*, 415–419.

(44) Kniprath, R.; Duhm, S.; Glowatzki, H.; Koch, N.; Rogaschewski, S.; Rabe, J. P.; Kirstein, S. Internal Structure of Nanoporous TiO₂/Polyion Thin Films Prepared by Layer-by-Layer Deposition. *Langmuir* **2007**, *23*, 9860–9865.

(45) Wu, Z.; Lee, D.; Rubner, M. F.; Cohen, R. E. Structural Color in Porous, Superhydrophilic, and Self-Cleaning SiO₂/TiO₂ Bragg Stacks. *Small* **2007**, *3*, 1445–1451.

(46) Lee, D.; Omolade, D.; Cohen, R. E.; Rubner, M. F. pH-Dependent Structure and Properties of TiO₂/SiO₂ Nanoparticle Multilayer Thin Films. *Chem. Mater.* **2007**, *19*, 1427–1433.

(47) Shimomura, H.; Gemici, Z.; Cohen, R. E.; Rubner, M. F. Layer-by-Layer-Assembled High-Performance Broadband Antireflection Coatings. *Appl. Mater. Interfaces* **2010**, *2*, 813–820.

(48) Braggeman, D. A. G. Calculation of Various Physical Constants of Heterogeneous Substances. Parts I, Dielectric Constant and Conductivity of Mixtures of Isotropic Substances. *Ann. Phys.* **1935**, *24*, 636–639.

(49) Erdogan, T. Fiber Grating Spectra. *J. Lightwave Technol.* **1997**, *15*, 1277–1294.

(50) Zhang, L.; Sun, J. Q. Layer-by-Layer Deposition of Polyelectrolyte Complexes for the Fabrication of Foam Coatings with High Loading Capacity. *Chem. Commun.* **2009**, 3901–3903.